A&A 490, 1005–1017 (2008)
DOI: 10.1051/0004-6361:200810590

Astronomy & Astrophysics

High-resolution radio continuum survey of M 33

III. Magnetic fields

F. S. Tabatabaei[1], M. Krause[1], A. Fletcher[2], and R. Beck[1]

[1] Max-Planck Institut für Radioastronomie, Auf dem Hügel 69, 53121 Bonn, Germany
e-mail: tabataba@mpifr-bonn.mpg.de
[2] School of Mathematics and Statistics, Newcastle University, Newcastle upon Tyne, NE1 7RU, UK

Received 14 July 2008 / Accepted 27 August 2008

ABSTRACT

Aims. We study the magnetic field structure, strength, and energy density in the Scd galaxy M 33.
Methods. Using the linearly polarized intensity and polarization angle data at 3.6, 6.2 and 20 cm, we determine variations of Faraday rotation and depolarization across M 33. We fit a 3D model of the regular magnetic field to the observed azimuthal distribution of polarization angles. We also analyze the spatial variation of depolarization across the galaxy.
Results. Faraday rotation, measured between 3.6 and 6.2 cm at an angular resolution of 3′ (0.7 kpc), shows more variation in the south than in the north of the galaxy. About 10% of the nonthermal emission from M 33 at 3.6 cm is polarized. High degrees of polarization of the synchrotron emission (>20%) and strong regular magnetic fields in the sky plane (≃6.6 μG) exist in-between two northern spiral arms. We estimate the average total and regular magnetic field strengths in M 33 as ≃6.4 and 2.5 μG, respectively. Under the assumption that the disk of M 33 is flat, the regular magnetic field consists of horizontal and vertical components: however the inferred vertical field may be partly due to a galactic warp. The horizontal field is represented by an axisymmetric ($m = 0$) mode from 1 to 3 kpc radius and a superposition of axisymmetric and bisymmetric ($m = 0 + 1$) modes from 3 to 5 kpc radius.
Conclusions. An excess of differential Faraday rotation in the southern half together with strong Faraday dispersion in the southern spiral arms seem to be responsible for the north-south asymmetry in the observed wavelength dependent depolarization. The presence of an axisymmetric $m = 0$ mode of the regular magnetic field in each ring suggests that a galactic dynamo is operating in M 33. The pitch angles of the spiral regular magnetic field are generally smaller than the pitch angles of the optical spiral arms but are twice as big as simple estimates based on the mean-field dynamo theory and M 33's rotation curve. Generation of interstellar magnetic fields from turbulent gas motion in M 33 is indicated by the equipartition of turbulent and magnetic energy densities.

Key words. galaxies: individual: M 33 – radio continuum: galaxies – galaxies: magnetic fields – galaxies: ISM

1. Introduction

Magnetic fields in galaxies can be traced by radio polarization measurements. The linearly polarized intensity gives information about the magnetic field strength and orientation in the plane of the sky, Faraday rotation measurements enable us to determine the magnetic field strength and direction along the line of sight and depolarizing effects can be sensitive to both components.

M 33, the nearest Scd galaxy at a distance of 840 kpc, with its large angular size (high-frequency radio continuum emission was detected in an area of 35′ × 40′, Tabatabaei et al. 2007c) and medium inclination of 56°, allows determination of the magnetic field components both parallel and perpendicular to the line of sight equally well. The first RM study of M 33, based on polarization observations at 11.1 and 21.1 cm (Beck 1979), suggested a bisymmetric regular magnetic field structure in the disk of M 33. Buczilowski & Beck (1991) confirmed the presence of this bisymmetric field using two further polarization maps at 6.3 and 17.4 cm. However, these results may be affected by weak polarized intensity and the consequent high uncertainty in RM in the southern half of M 33, due to the low-resolution (7.7′ or 1.8 kpc) and low-sensitivity of the observations.

Our recent observations of this galaxy provided high-sensitivity and high-resolution (3′ ≃ 0.7 kpc) maps of total power and linearly polarized intensity at 3.6, 6.2, and 20 cm presented by Tabatabaei et al. (2007c). These data are ideal to study the rotation measure (RM), magnetic fields (structure and strength), and depolarization effects in detail.

Tabatabaei et al. (2007c) found a north-south asymmetry in the polarization distribution that is wavelength dependent, indicating a possible north-south asymmetry in Faraday depolarization. Investigation of this possibility requires a knowledge of the distribution of RM, the turbulent magnetic field and thermal electron density in the galaxy. Furthermore, depolarization is best quantified using the nonthermal degree of polarization rather than the fraction of the total radio emission that is polarized. Tabatabaei et al. (2007b) developed a new method to separate the thermal and nonthermal components of the radio continuum emission from M 33 which yielded maps of the nonthermal synchrotron emission and the synchrotron spectral index variations across the galaxy (Tabatabaei et al. 2007a). The nonthermal maps are used in this paper to determine the nonthermal degree of polarization at different wavelengths, and hence to study how the radio continuum emission from different parts of M 33 is depolarized.

By combining an analysis of multi-wavelength polarization angles with modeling of the wavelength dependent depolarization, Fletcher et al. (2004) and Berkhuijsen et al. (1997) derived the 3D regular magnetic field structures in M 31 and M 51, respectively. The high sensitivity of our new observations allows a similar study for M 33.

We first determine the nonthermal degree of polarization using the new nonthermal maps (Sect. 2). Then we calculate a map of the RM intrinsic to M 33 with a spatial resolution of 3′ or 0.7 kpc and probe its mean value in rings in the galactic plane in Sect. 3. The regular magnetic field structure is derived in Sect. 4 and the estimated strengths are presented. We derive a map for the observed depolarization and discuss the possible physical causes of depolarization sources in Sect. 5. Furthermore, we discuss the resulting vertical fields and pitch angles in Sect. 6. The estimated energy density of the magnetic field is compared to the thermal and turbulent energy densities of the interstellar gas.

2. Nonthermal degree of polarization

The degree to which synchrotron emission is polarized reflects the degree of coherent structure in the magnetic field within one beam-area; a purely regular magnetic field will produce about 75%[1] fractional polarization of synchrotron emission. The quantity of interest is the degree of polarization of the synchrotron emission or "nonthermal degree of polarization", $P_{\rm nth} = PI/I_{\rm nth}$, where PI is the intensity of the linearly polarized emission and $I_{\rm nth}$ is the intensity of the nonthermal emission.

Since we observe the total intensity I, which consists of both nonthermal $I_{\rm nth}$ and thermal $I_{\rm th}$ intensities at cm wavelengths, $P_{\rm nth}$ cannot be calculated straightforwardly. To date, $P_{\rm nth}$ has been estimated by assuming either a fixed ratio $I_{\rm th}/I$ or $I_{\rm nth}$ has been derived assuming a fixed spectral index of the synchrotron emission. Here we use a new, more robust method for determining the distribution of $I_{\rm nth}$ by correcting Hα maps for dust extinction, using multi-frequency infra-red maps at the same resolution, and thus independently estimating $I_{\rm th}$ (Tabatabaei et al. 2007b). Using the PI maps of Tabatabaei et al. (2007c) and the nonthermal maps obtained by Tabatabaei et al. (2007b), we derived maps of $P_{\rm nth}$ at different wavelengths.

Figure 1 shows $P_{\rm nth}$ at 3.6 cm. High nonthermal degrees of polarization ($P_{\rm nth} > 30\%$) are found in several patches of M 33, with the most extended region of high $P_{\rm nth}$ in the northern part of the magnetic filament identified by Tabatabaei et al. (2007c), inside the second contour at Dec > 30°54′ in Fig. 1. The high $P_{\rm nth}$ also exist at 6.2 cm in these regions.

Integrating the polarized and nonthermal intensity maps in the galactic plane out to a galactocentric radius of $R \leq 7.5$ kpc, we obtained the flux densities of the nonthermal $S_{\rm nth}$ and linearly polarized S_{PI} emission along with the average nonthermal degree of polarization $\bar{P}_{\rm nth} = S_{PI}/S_{\rm nth}$. Table 1 gives $S_{\rm nth}$, S_{PI}, and $\bar{P}_{\rm nth}$ at different wavelengths, all at the same angular resolution of 180″. At 3.6 and 6.2 cm, $\bar{P}_{\rm nth}$ is the same, demonstrating that Faraday depolarization effects are not significant at these wavelengths: the weaker S_{PI} at 3.6 cm is due to lower synchrotron emissivity, as expected from the power-law behavior of synchrotron emission with respect to frequency. However, Faraday depolarization effects are possibly important at 20 cm reducing $\bar{P}_{\rm nth}$.

[1] If a nonthermal spectral index of $\alpha_n = 1$ is used.

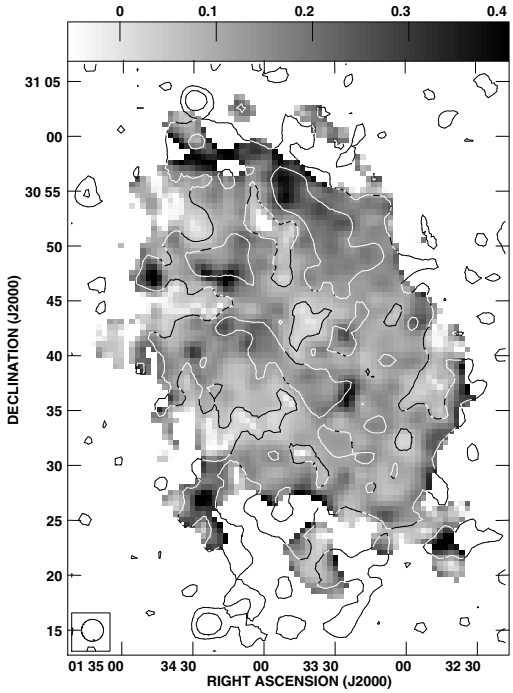

Fig. 1. Nonthermal degree of polarization at 3.6 cm, with an angular resolution of 2′ (the beam area is shown in *the left-hand corner*). Overlayed are contours of the linearly polarized intensity at 3.6 cm with levels of 0.1 and 0.3 mJy/beam.

Table 1. Integrated nonthermal flux densities and average nonthermal degree of polarization at 180″.

λ (cm)	$S_{\rm nth}$ (mJy)	S_{PI} (mJy)	$\bar{P}_{\rm nth}$ %
3.6	370 ± 60	38 ± 4	10.3 ± 2.0
6.2	696 ± 110	79 ± 5	11.3 ± 1.9
20	1740 ± 65	115 ± 10	6.6 ± 0.6

3. Rotation measures

When linearly polarized radio waves propagate in a magneto-ionic medium, their polarization vector is systematically rotated. The amount of Faraday rotation depends on the wavelength (λ) of the radio emission, the strength of the magnetic field along the line of sight (that is the regular field in the line of sight $B_{\rm reg\parallel}$), and the number density of thermal electrons ($n_{\rm e}$) along the line of sight (l):

$$\frac{\Delta\phi}{\rm rad} = 0.81\left(\frac{\lambda}{\rm m}\right)^2 \int_0^{\frac{L}{\rm pc}} \left(\frac{B_{\rm reg\parallel}}{\mu\rm G}\right)\left(\frac{n_{\rm e}}{\rm cm^{-3}}\right) {\rm d}\left(\frac{l}{\rm pc}\right), = 0.81\lambda^2\mathcal{R} \quad (1)$$

where L is the path length through the magneto-ionic medium. Hence, the measured polarization angle ($\phi = \frac{1}{2}\arctan\frac{U}{Q}$) differs from the intrinsic polarization angle ($\phi_{\rm i}$) as

$$\phi - \phi_{\rm i} = \Delta\phi \equiv \lambda^2\,\mathcal{R}. \quad (2)$$

When Faraday depolarization is small (the Faraday-thin condition), $\mathcal{R}$ does not depend on wavelength (Sokoloff et al. 1998) and an estimate for $\mathcal{R}$ can be obtained from measurements of the polarization angles at two wavelengths:

$$\frac{\rm RM}{\rm rad\,m^{-2}} = \frac{(\phi_1/{\rm rad}) - (\phi_2/{\rm rad})}{\left(\frac{\lambda_1}{\rm m}\right)^2 - \left(\frac{\lambda_2}{\rm m}\right)^2}. \quad (3)$$

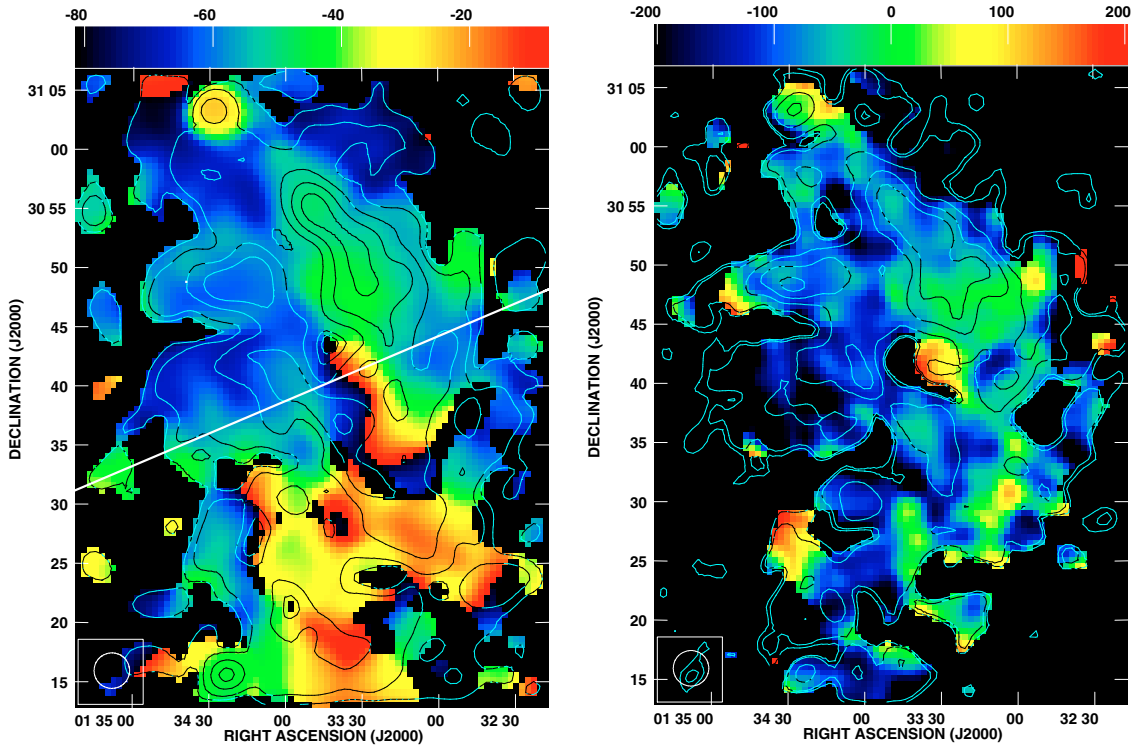

Fig. 2. *Left*: observed rotation measure map of M 33 (rad m^{-2}) between 3.6 and 20 cm with contours of 3.6 cm polarized intensity. Contour levels are 0.1, 0.2, 0.4, 0.6, 0.8 mJy/beam. *Right*: observed rotation measure between 3.6 and 6.2 cm with contours of 6.2 cm polarized intensity. Contour levels are 0.3, 0.4, 0.8, 1.2, 1.6 mJy/beam. The angular resolution in both maps is 3′ (the beam area is shown in *the left-hand corners*). The straight line in *the left panel* shows the minor axis of M 33.

In this definition, the unknown intrinsic polarization angle of the source (or sources along the line of sight) cancels out. A positive RM indicates that $B_{\rm reg||}$ points towards us.

Part of the measured RM is due to the interstellar medium of M 33 (intrinsic RM or $\rm RM_i$); the rest is due to the Galactic foreground medium ($\rm RM_{fg}$), $\rm RM = RM_i + RM_{fg}$. The foreground rotation measure in the direction of M 33 is mainly caused by the extended Galactic magnetic bubble identified as region *A* by Simard-Normandin & Kronberg (1980). Assuming that the intrinsic contributions of the extragalactic sources 3C 41, 3C 42, and 3C 48 (in a 5° × 5° region around M 33) themselves cancel out and the intragalactic contribution is negligible, Broten et al. (1988) and Tabara & Inoue (1980) found a foreground rotation measure of −57 ± 10 rad m^{-2} for those sources. For the polarized sources in the 2° × 2° M 33 field, Buczilowski & Beck (1991) found a foreground RM of −55 ± 10 rad m^{-2}. About the same value was obtained by Johnston-Hollitt et al. (2004). In the following we use $\rm RM_{fg} = -55$ rad m^{-2}.

Using the polarization data of Tabatabaei et al. (2007c, where $PI > 2\sigma$ noise level), we first obtained the distribution of RM between 3.6 and 20 cm across M 33 (Fig. 2, left panel), showing a smooth distribution of RM in the northern half of the galaxy. However, stronger and more abrupt fluctuations in RM occur in the southern half of the galaxy, which are not due to the $\pm n\,73$ rad m^{-2} ambiguity in RM between these wavelengths ($\pm n\pi/|\lambda_1^2 - \lambda_2^2|$). Weak polarized emission in the southern half at 20 cm (presented in Tabatabaei et al. 2007c) can be linked to these RM variations. Between 3.6 and 6.2 cm, RM varies less than between 3.6 and 20 cm in the south of the galaxy (Fig. 2, right panel). This indicates that the relation between $\Delta\phi$ and λ^{-2} in Eq. (2) is not linear over the interval between 3.6 and 20 cm due to Faraday depolarization at 20 cm in the south of M 33 and so RM measured at these wavelengths is not a good estimator of $\mathcal{R}$.

Figure 3 shows $\rm RM_i$ between 3.6 and 6.2 cm which varies in a range including both positive and negative values. Comparing $\rm RM_i$ with the overlayed contours of PI[2], $\rm RM_i$ seems to vary more smoothly in regions of high PI. The apparent agreement between the ordered magnetic field in the plane of the sky and the regular magnetic field in the line of sight is clearest in the north and along the minor axis and is best visible in the magnetic filament between the arms IV and V in the north-west of M 33 (Fig. 4, see also Tabatabaei et al. 2007c) where $\rm RM_i$ shows small variation within the PI contours. This indicates that the ordered magnetic field in this region is mainly regular. Sign variations of $\rm RM_i$ are more frequent (arising locally) in the southern half, where there is no correlation with PI, than in the northern half of the galaxy. This indicates that the regular magnetic field is more affected by local phenomena (like starforming activity, e.g. see Tabatabaei et al. 2007c) in the south than in the north of the galaxy. The local $\rm RM_i$ variations between large positive and negative values may represent loop-like magnetic field structures going up from and down to the plane (e.g. Parker loops). This is particularly seen in the central part of the galaxy as well as regions in the southern arm II S (Fig. 4).

Figure 3 also shows that the magnetic field is directed towards us on the western minor axis (at azimuth $\theta \approx 110°$ and $\theta \approx 290°$), but has an opposite direction on the eastern side. The large $\rm RM_i$ values in regions with small electron density, e.g. on the eastern and western minor axis and in a clumpy

[2] Note that PI is related to the magnetic field in the plane of the sky that is a combination of both a mean field (or coherent regular field) and anisotropic (compressed or sheared) random fields. $\rm RM_i$ is related to only coherent regular field along the line of sight.

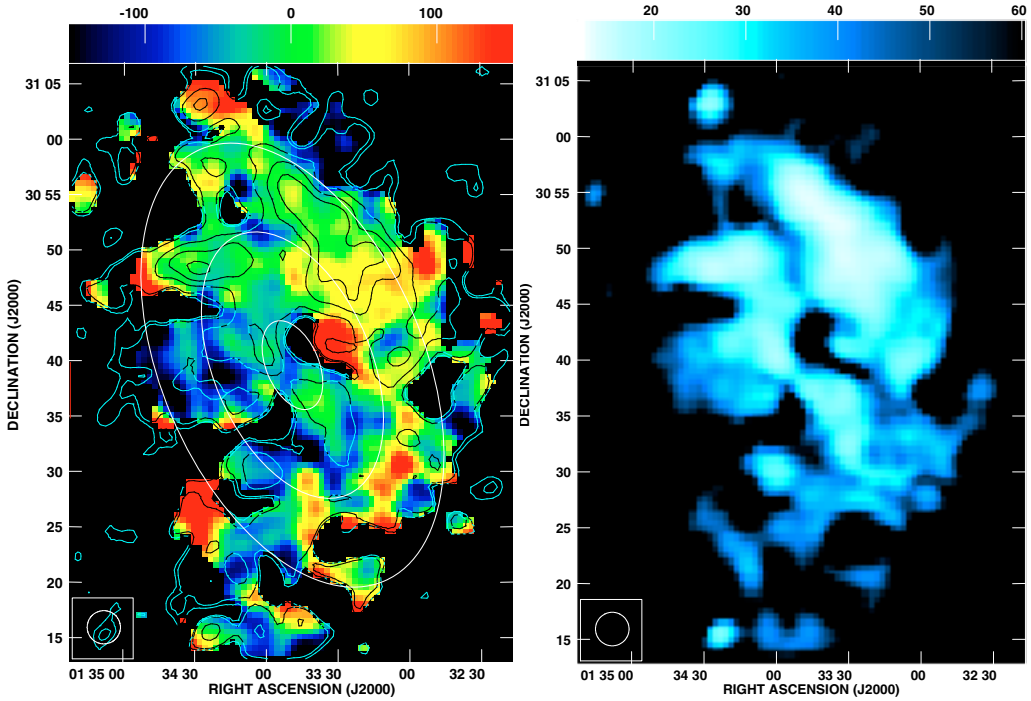

Fig. 3. *Left*: rotation measure map of M 33 (rad m^{-2}) between 3.6 and 6.2 cm after correction for the foreground $\mathrm{RM_{fg}} = -55$ rad m^{-2}, with an angular resolution of 3′ (the beam area is shown in *the left-hand corner*). Overlayed are contours of 6.2 cm polarized intensity. Contour levels are 0.3, 0.4, 0.8, 1.2, 1.6, 3.2, 6.4 mJy/beam. Also shown are rings at 1, 3, and 5 kpc radii as used in Sect. 4. *Right*: the distribution of the estimated error in RM is shown in *the right panel*.

distribution in the central south near the major axis with 30°25′ < Dec < 30°30′ (Tabatabaei et al. 2007b), indicates a strong magnetic field along the line of sight and/or large path length through the magneto-ionic medium. Considerable Faraday rotation measured on the eastern and western minor axis hints at a deviation from a purely toroidal structure for the large-scale magnetic field (Krause 1990; Beck et al. 1996). Furthermore, along with the magnetic field parallel to the disk, the presence of a field component vertical to the galactic disk is indicated in kpc-scale regions of large $\mathrm{RM_i}$ but small n_e values. The existence of the vertical magnetic field in M 33 (that is strong near the major axis) is shown in Sect. 4.

4. The magnetic field

4.1. The regular magnetic field structure

The λ3.6 cm polarization angles were corrected for Faraday rotation and rotated by 90° to obtain the intrinsic orientation of the regular magnetic field component in the plane of the sky ($B_{\mathrm{reg}\perp}$). Figure 4 shows the derived $B_{\mathrm{reg}\perp}$ superimposed on an optical image of M 33. The orientation of $B_{\mathrm{reg}\perp}$ shows a spiral magnetic field pattern with a similar pitch angle to the optical arms in the north and south, but larger pitch angles in the east and west of the galaxy.

The apparent continuity of the regular magnetic field straight through the center of M 33 is remarkable. The Faraday rotation map (Fig. 3) shows that the field is oppositely directed on the east and west sides of the center. Unfortunately the current data lack the resolution to investigate the field properties in this region further.

The behavior of $B_{\mathrm{reg}\perp}$ along the minor axis ($\theta \approx 110°$, $\theta \approx 290°$) is also informative. $B_{\mathrm{reg}\perp}$ on the minor axis clearly has a strong radial component (Fig. 4). If we assume that B_{reg} lies solely in the disc, so that $B_{\mathrm{reg}\parallel}$ is produced by the galaxy's inclination (i.e. $B_z = 0$), then the change of sign in RM along the minor axis (Fig. 3) indicates that the direction of the radial component of $\boldsymbol{B}_{\mathrm{reg}}$ is towards the center on both sides of the minor axis. This means that the dominant azimuthal mode of B_{reg} cannot be the bisymmetric $m = 1$ mode suggested by earlier studies (Beck 1979; Buczilowski & Beck 1991): we expect the dominant mode to be even.

In order to identify the 3D structure of the *regular* magnetic field B_{reg} we fit a parameterized model of B_{reg} to the observed polarization angles at different wavelengths using the method successfully employed by Berkhuijsen et al. (1997) and Fletcher et al. (2004) to determine the magnetic field structures of M 51 and M 31 respectively.

At each wavelength the maps in the Stokes parameters Q and U are averaged in sectors of 10° opening angle and 2 kpc radial width in the range $1 \le r \le 5$ kpc. The size of the sectors is chosen so that the area of the smallest sector is roughly equivalent to one beam-area. We also take care that the standard deviation of the polarization angle in each sector is greater than the noise (if the sector sizes are too small then fluctuations in angle due to noise can be larger than the standard deviation). Then the average Q and U intensities are combined to give the average polarization angle $\psi = 0.5 \arctan U/Q$ and the average polarized emission intensity $PI \sqrt{(Q^2 + U^2)}$ in each sector.

The observed polarization angles are related to the underlying properties of the regular magnetic field in M 33 by[3]

$$\psi = \psi_0(B_{\mathrm{reg}\perp}) + \lambda^2 \mathrm{RM_i}(B_{\mathrm{reg}\parallel}) + \lambda^2\, \mathrm{RM_{fg}}, \quad (4)$$

[3] Note that we choose different symbols for the average polarization angle ϕ and the average polarization angle in sectors ψ.

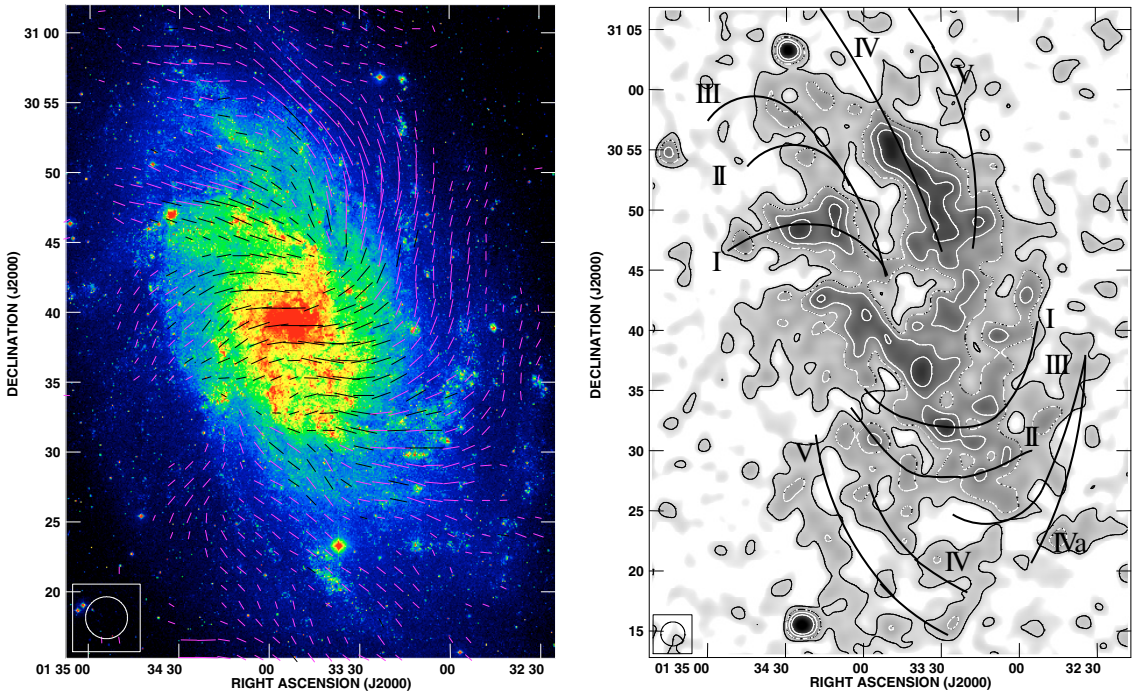

Fig. 4. *Left*: optical image (*B*-band, taken from the STScI Digitized Sky Survey) of M 33 with overlayed vectors of intrinsic magnetic field in the sky-plane with 3′ angular resolution. The length gives the polarized intensity at 3.6 cm, where 1′ is equivalent to 0.37 mJy/beam. *Right*: a sketch of the optical arms (Sandage & Humphreys 1980) overlayed on the linearly polarized intensity with an angular resolution of 2′ (contours and grey scale) at 3.6 cm (see Tabatabaei et al. 2007c).

where ψ_0 is the intrinsic angle of polarized emission, $\mathrm{RM_i}$ is the Faraday rotation experienced by a photon as it passes through the magneto-ionic medium of M 33 and $\mathrm{RM_{fg}}$ is foreground Faraday rotation due to the Milky Way. $B_{\mathrm{reg}\perp}$ is the component of the regular magnetic field of M 33 that lies in the sky-plane and $B_{\mathrm{reg}\parallel}$ the component directed along the line-of-sight.

The cylindrical components of the regular field in the disk of M 33 $\boldsymbol{B}_{\mathrm{reg}} = (B_r,\ B_\theta,\ B_z)$ can be represented in terms of the Fourier series in the azimuthal angle θ:

$$
\begin{aligned}
B_r &= B_0 \sin p_0 + B_1 \sin p_1 \cos(\theta - \beta_1) \\
&\quad + B_2 \sin p_2 \cos 2(\theta - \beta_2), \\
B_\theta &= B_0 \cos p_0 + B_1 \cos p_1 \cos(\theta - \beta_1) \\
&\quad + B_2 \cos p_2 \cos 2(\theta - \beta_2), \\
B_z &= B_{z0} + B_{z1} \cos(\theta - \beta_{z1}) + B_{z2} \cos 2(\theta - \beta_{z2}),
\end{aligned} \tag{5}
$$

where B_m and B_{zm} are the amplitude of the mode with azimuthal wave number m in the horizontal and vertical fields, p_m is the constant pitch angle of the mth horizontal Fourier mode (i.e. the angle between the field and the local circumference) and β_m and β_{zm} are the azimuths where the non-axisymmetric modes are maximum. The amplitudes of the Fourier modes are obtained in terms of the variables B_m in units of $\mathrm{rad\,m^{-2}}$: in order to obtain amplitudes in Gauss independent information is required about the average thermal electron density and disc scale-height. Useful equations describing how $B_{\mathrm{reg}\perp}$ and $B_{\mathrm{reg}\parallel}$ are related to the field components of Eq. (5) can be found in Appendix A of Berkhuijsen et al. (1997).

Using Eqs. (4) and (5), and taking into account the inclination (56°) and major-axis orientation (23°) of M 33, we fit the three-dimensional $\boldsymbol{B}_{\mathrm{reg}}$ to all of the observed polarization angles in a ring by minimizing the residual

$$
S = \sum_{\lambda,n} \left[\frac{\psi_n - \psi(\theta_n)}{\sigma_n} \right]^2, \tag{6}
$$

where ψ_n is the observed angle of polarization, $\psi(\theta_n)$ the modelled angle in the sector centred on azimuth θ_n and σ_n are the observational errors. The Fisher test is used to ensure that the fits at each wavelength are statistically equally good (see Appendix B in Berkhuijsen et al. 1997). Errors in the fit parameters are estimated from the region of parameter space where $S \leq \chi^2$ at the 2σ level.

4.2. Results of fitting

We applied the method described in Sect. 4 to the polarization maps at 3.6 and 6.2 cm. A preliminary examination of the data at all three wavelengths showed that the 20 cm polarization angles do not have the same $\psi \propto \lambda^2$ Faraday rotation dependence as the angles at 3.6 and 6.2 cm. This is most probably because the 20 cm signal is strongly depolarized by Faraday effects (see Sect. 5) and so only photons from an upper layer of the emitting region are detected in polarization. If the depolarization is constant at a given radius, a "depth" parameter can be used to take account of this effect (Berkhuijsen et al. 1997; Fletcher et al. 2004). However, in the case of M 33 depolarization is strongly asymmetric (Fig. 11) and this method does not lead to consistent results: we therefore work only with the polarization angles at 3.6 and 6.2 cm to model the regular magnetic field.

We fixed the foreground Faraday rotation, $\mathrm{RM_{fg}}$ in Eq. (4), to $-55\ \mathrm{rad\,m^{-2}}$ (see Sect. 3). For each ring we found more than one statistically good fit to the observed polarization angles, three different fits in the 1−3 kpc ring and two fits in the

Table 2. Parameters of the fitted models and their 2σ errors. RM_{fg} is the Faraday rotation measure arising in the Milky Way, B_m and p_m are the amplitude and pitch angle of the mode with wave number m, and β_m is the azimuth where a mode with azimuthal wave number m is maximum. The minimum value of the residual S and the value of χ^2 are shown for each model in the bottom lines. The combination of azimuthal modes of $m = 0 + z0 + z1$ and $m = 0 + 1 + z1$ can best reproduce the observed polarized intensity in the 1–3 and 3–5 kpc rings, respectively (Figs. 5 and 6).

	Units	Radial range (kpc)				
			1–3		3–5	
RM_{fg}	rad m^{-2}	-55 ± 45	-55^{+6}_{-9}	-55^{+30}_{-59}	-55^{+30}_{-60}	-55 ± 19
B_0	rad m^{-2}	-30^{+11}_{-20}	-69 ± 4	-14 ± 2	-13 ± 3	-103 ± 9
p_0	deg	48 ± 12	51 ± 2	42 ± 4	42^{+1}_{-7}	41 ± 2
B_1	rad m^{-2}			-12 ± 3	-9 ± 2	
p_1	deg			28^{+1}_{-9}	14^{+11}_{-7}	
β_1	deg			-56^{+12}_{-1}	-67^{+22}_{-39}	
B_2	rad m^{-2}		-41 ± 3			-67 ± 6
p_2	deg		-87 ± 6			-103 ± 8
β_2	deg		-12 ± 3			-22 ± 4
B_{z0}	rad m^{-2}	-14 ± 15				
B_{z1}	rad m^{-2}	-52^{+22}_{-35}		-16 ± 5	-14 ± 4	
β_{z1}	deg	32^{+21}_{-16}		24^{+1}_{-10}	9 ± 9	
m		$0 + z0 + z1$	$0 + 2$	$0 + 1 + z1$	$0 + 1 + z1$	$0 + 2$
S		56	83	57	57	82
χ^2		85	85	84	84	85

3–5 kpc ring; the fitted parameters are shown in Table 2. All of the fits require the presence of more than one azimuthal Fourier mode and have two common characteristics: the presence of an $m = 0$ mode that has a significant amplitude and that the pitch angle of the $m = 0$ mode is in the range $40° \lesssim p \lesssim 50°$. The reason why several equally good fits are found is the rather weak large-scale intrinsic rotation measure, i.e. the amplitude of systematic rotation measure variations is rather low compared to local fluctuations. This is a sign that the regular magnetic field of M 33 is not as well-ordered and strong, relative to the small-scale field, as that of, for example, M 31 (Fletcher et al. 2004).

The model regular magnetic field given by Eq. (5) is fitted to the observed polarization *angles*, in order to obtain the results shown in Table 2. Since we have not made use of the observed polarized *intensity* we can try to use this to select the best regular magnetic field model for each of the two rings from the fits given in Table 2. We compare the predicted azimuthal pattern of polarized intensity from the model fields with the observed polarized intensity (PI) at 6.2 (Faraday depolarization effects are negligible at 6.2 cm and emissivity is higher than at 3.6 cm due to the spectral index, thus giving a stronger signal). The model described by Eq. (5) is not designed to reproduce the observed PI so we cannot make meaningful statistical assessments about the relative merits of the different fits in a given ring. But we can judge whether or not the fits are better or worse than each other in explaining the location of the main maxima and minima in the observed pattern of PI and so try to select a preferred model field for each ring.

Figures 5 and 6 shows the square of the predicted plane-of-sky regular magnetic field $B^2_{reg\perp}$ for each of the fits given in Table 2 and the observed 6.2 cm polarized intensity, both normalized to avoid having to use a prescription for the poorly known synchrotron emissivity. In the case of energy equipartition between cosmic rays and magnetic fields the polarized intensity would be proportional to a higher power of $B_{reg\perp}$ than 2 and maxima would be more pronounced.

In the 1–3 kpc ring, the model field with the components of $m = 0 + z0 + z1$[4] (Fig. 5a) reproduces the broad features of the observed polarized emission better than the models using the modes $m = 0 + 1 + z1$ (Fig. 5b) and $m = 0 + 2$ (Fig. 5c). The match to the observed PI is far from perfect in Fig. 5a but this is the only model field that can account for the strong excess of PI at 6 cm in the northern half of the disc at these radii. In the 3–5 kpc ring the fit using $m = 0 + 1 + z1$ (Fig. 6, top) is better at reproducing the general pattern of polarized emission at 6 cm than the other statistically good fit using $m = 0 + 2$ (Fig. 6, bottom). Again, the match to observations is not perfect, but the model with $m = 0 + 2$ would produce a strong maximum in PI at $\theta \sim 90°$ that is not observed.

To summarize: we select the statistically good fit using the modes $m = 0 + z0 + z1$ in the 1–3 kpc ring and that using $m = 0 + 1 + z1$ in the 3–5 kpc ring as being the best descriptions of the regular magnetic field in M 33 (the parameters of these two preferred fits are given in Cols. 3 and 6 of Table 2). Our reason is that the $B^2_{reg\perp}$ produced by these models produces a much closer match to the observed pattern of PI at 6.2 cm than other statistically good models. Figure 7 shows the regular magnetic field in a face-on view of the galaxy (thus the vertical field components cannot be seen).

4.3. The equipartition magnetic field strengths

The strengths of the total magnetic field B_{tot} and its regular component B_{reg} can be found from the total synchrotron intensity and its degree of linear polarization P_{nth}. Assuming equipartition between the energy densities of the magnetic field and cosmic rays ($\varepsilon_{CR} = \varepsilon_{B_{tot}} = B^2_{tot}/8\pi$),

$$B_{tot} = \left[\frac{4\pi(2\alpha_n + 1)\, K'\, I_n\, E_p^{1-2\alpha_n} \left(\frac{\nu}{2c_1}\right)^{\alpha_n}}{(2\alpha_n - 1)\, c_2(\alpha_n)\, L\, c_3} \right]^{\frac{1}{\alpha_n + 3}} \quad (7)$$

[4] $z0$ and $z1$ are the first and second Fourier modes of the vertical field.

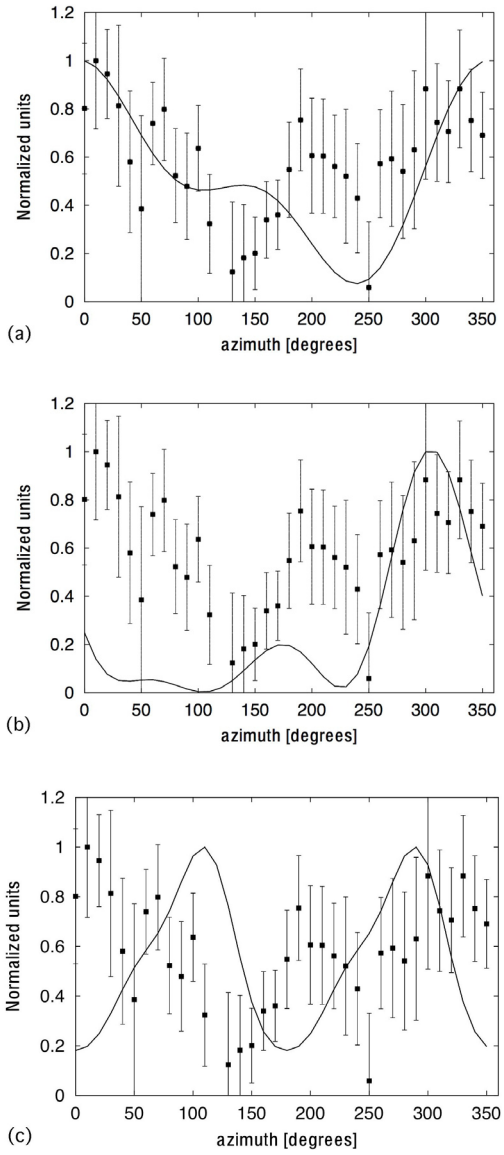

Fig. 5. Polarized intensity (PI) at 6 cm in the 1−3 kpc ring, observed (points with error bars) and expected from the modelled regular magnetic field (lines) with $PI \propto B^2_{\mathrm{reg}\perp}$ given by the different fits shown in Table 2. **a)** Using a fitted regular magnetic field containing the modes $m = 0 + z0 + z1$. **b)** As **a)** but for the fit containing the modes $m = 0 + 1 + z1$. **c)** as **a)** but for the fit containing the modes $m = 0 + 2$.

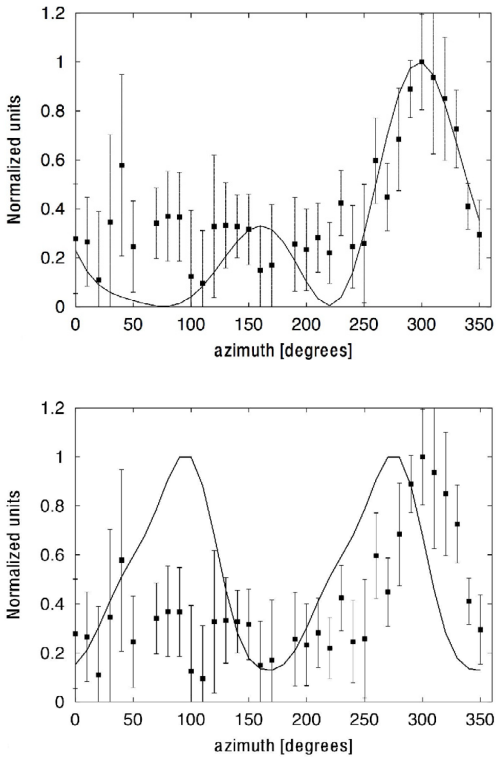

Fig. 6. As Fig. 5 but for the 3−5 kpc ring using a fitted regular magnetic field containing the modes $m = 0 + 1 + z1$ (*top*) and $m = 0 + 2$ (*bottom*).

(Beck & Krause 2005), where $K' = K + 1$ with K the ratio between the number densities of cosmic ray protons and electrons, I_n is the nonthermal intensity, L the pathlength through the synchrotron emitting medium, and α_n the mean synchrotron spectral index. $E_\mathrm{p} = 938.28\,\mathrm{MeV} = 1.50 \times 10^{-3}$ erg is the proton rest energy and

$$c_1 = 3e/(4\pi {m_\mathrm{e}}^3 c^5) = \frac{6.26428 \times 10^{18}}{\mathrm{erg}^2\ \mathrm{s\ G}},$$

$$c_2(\alpha_n) = \frac{1}{4} c_3\ (\alpha_n + 5/3)\,/(\alpha_n + 1)\,\Gamma[(3\alpha_n + 1)/6] \times \Gamma[(3\alpha_n + 5)/6].$$

For a region where the field is completely regular and has a constant inclination i with respect to the sky plane ($i = 0^\mathrm{o}$ is the face-on view), $c_3 = [\cos(i)]^{(\alpha_n+1)}$. If the field is completely turbulent and has an isotropic angle distribution in three dimensions, $c_3 = (2/3)^{(\alpha_n+1)/2}$. If the synchrotron intensity is averaged over a large volume, $[\cos(i)]^{(\alpha_n+1)}$ has to be replaced by its average over all occurring values of i.

The strength of the regular magnetic field in the plane of the sky can be estimated from the observed nonthermal degree of polarization (Segalovitz et al. 1976):

$$P_\mathrm{nth} = \left(\frac{3\gamma + 3}{3\gamma + 7}\right) \times \left[1 + \frac{(1-q)\,\pi^{1/2}\,\Gamma[(\gamma+5)/4]}{2q\Gamma[(\gamma+7)/4]F(i)}\right]^{-1},$$

$$F(i) = \frac{1}{2\pi} \int_0^{2\pi} \left(1 - \sin^2 i\,\sin^2\theta\right)^{(\gamma+1)/4} \mathrm{d}\theta, \qquad (8)$$

with $B_\mathrm{reg}/\,B_\mathrm{tur} = q^{2/(1+\gamma)}$, $\gamma = 2\alpha_n + 1$, and θ the azimuthal angle (B_tur is the turbulent magnetic field). This formula assumes that the regular magnetic field has a single orientation, is parallel to the disk and, taken over the galaxy as a whole, has no further preferential orientation with respect to any fixed direction in space.

The determined average values of I_n, α_n, and P_nth with the assumed values of K ($\simeq$100) and L ($\simeq$1 kpc/cos i) lead to $B_\mathrm{tot} = 6.4 \pm 0.5\ \mu$G and $B_\mathrm{reg} = 2.5 \pm 1.0\ \mu$G for the disk of M 33 ($R < 7.5$ kpc). The strongest regular magnetic field is found in between the northern arms IV N and V N (in the magnetic filament) with $B_\mathrm{reg} \simeq 6.6\ \mu$G where $B_\mathrm{tot} \simeq 8.3\ \mu$G.

The regular magnetic field strength estimated from the mean rotation measure in sectors and assuming $n_\mathrm{e} \simeq 0.03\ \mathrm{cm}^{-3}$ (see Sect. 5) is $1.4^{+0.9}_{-0.5}\ \mu$G and $0.6 \pm 0.1\ \mu$G in the 1−3 kpc and 3−5 kpc rings, respectively. In the 1−3 kpc ring, the regular field strength is consistent with that estimated from the equipartition

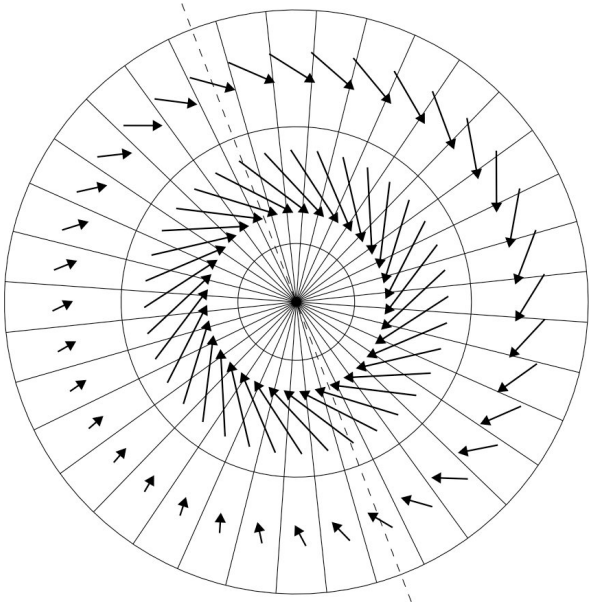

Fig. 7. The regular magnetic field described by our favoured fitted model (see Sect. 4.2 for details). The galaxy has been deprojected into a face-on view, so only the disk-plane components of the magnetic field are shown; the vertical components are not visible. The dashed line shows the major axis of M 33, with north to the top. The ring boundaries are at 1, 3 and 5 kpc.

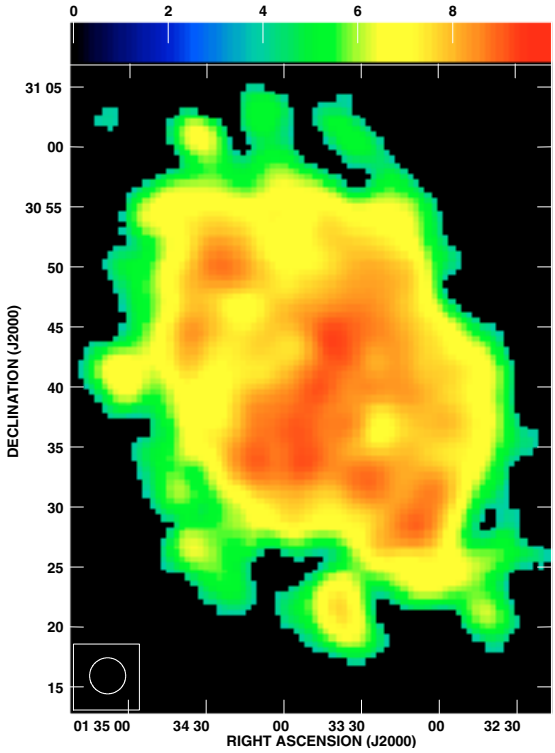

Fig. 8. Distribution of the turbulent magnetic field strength, $B_{\rm tur}$ (μG), in M 33 with an angular resolution of 3′ (the beam area is shown in *the left-hand corner*). Contour levels are 4.1, 5.0, 5.8, 6.6, 7.5 μG.

assumption, while it is much smaller in the 3–5 kpc ring. The more frequent RM variations in both amplitude and sign in the second ring (see Fig. 3) indicate a line-of-sight field component with many reversals and a small mean RM within each sector, whereas the field component in the sky plane causes significant polarized emission (which is insensitive to the field reversals).

The equipartition total magnetic field strength of 6 ± 0.5 μG is slightly higher than the total field obtained by Buczilowski & Beck (1991), 4 ± 1 μG, assuming the minimum total energy requirement of the disk-like synchrotron source. This is not surprising because a difference of ≃20% is expected between the minimum and equipartition magnetic field strengths for field strengths of about 5 μG (Beck & Krause 2005). Furthermore, the mean nonthermal fraction from the standard thermal/nonthermal separation method is lower than that from the new method (Tabatabaei et al. 2007b), resulting in a weaker equipartition magnetic field.

As the polarized intensity (PI/0.75, corrected for the maximum fractional polarization in a completely regular field) is related to the regular magnetic field strength, and the nonthermal intensity (I_n) to the total magnetic field strength in the plane of the sky, $I_n - (PI/0.75)$ gives the nonthermal emission due to the turbulent magnetic field $B_{\rm tur}$. Using this intensity with Eq. (7) and assuming a completely turbulent field yields the distribution of $B_{\rm tur}$ across the galaxy. Figure 8 shows strong $B_{\rm tur}$ (>7 μG) in the central region of the galaxy, the arm I S, and parts of the northern arm I N.

Using the mean synchrotron flux density, synchrotron spectral index, and degree of polarization in rings, we also derive the average field strengths in rings. Figure 9 shows some fluctuations but no systematic increase or decrease of these strengths with galactocentric radius. The small bump at $4.5 < R < 5.5$ kpc is due to M 33's magnetic filament.

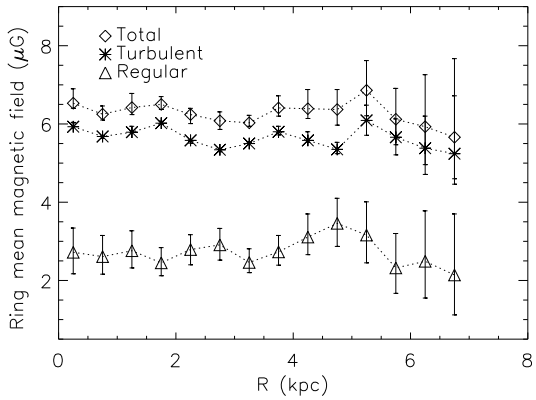

Fig. 9. Variation of the mean total, regular, and turbulent magnetic field strengths in rings of 500 pc width with galactocentric radius.

5. Depolarization

The depolarization observed at a certain wavelength is defined as the ratio of the nonthermal degree of linear polarization $P_{\rm nth}$ and the theoretical maximum value p_0 (75% for $\alpha_n = 1$). Generally, depolarization may be caused by instrumental effects due to the bandwidth and beamwidth of the observations or by the wavelength-dependent Faraday depolarization. Bandwidth depolarization occurs when the polarization angles vary across the frequency band, reducing the observed amount of polarized emission. It is given by $\mathrm{sinc}\,(2\,\mathrm{RM}\,\lambda^2\,\delta\nu/\nu)$, where $\delta\nu$ is the bandwidth of the observations (e.g. Reich 2006). In our study, the wavelengths, bandwidths and RM values lead to a negligible bandwidth depolarization. Beamwidth depolarization occurs when polarization vectors of different orientation are unresolved in the telescope beam. In order to compensate for this effect,

the ratio of the nonthermal degree of polarization at two wavelengths is used at a same angular resolution,

$$\mathrm{DP}_{\lambda_2/\lambda_1} = \frac{P^{\lambda_2}_{\mathrm{nth}}}{P^{\lambda_1}_{\mathrm{nth}}}, \quad (9)$$

where $\lambda_2 > \lambda_1$. The observed depolarization $\mathrm{DP}_{\lambda_2/\lambda_1}$, that is only wavelength *dependent*, is called the Faraday depolarization.

We derived the depolarization $\mathrm{DP}_{20/3.6}$ using the maps of nonthermal and polarized intensity at 20 and 3.6 cm at the same angular resolution of 180″ (Fig. 11, top panel). The southern half of the galaxy is highly depolarized compared to the northern half. While $\mathrm{DP}_{20/3.6}$ changes between 0.0 and 0.5 in the south, it varies between 0.3 and 1.0 in the north. Considerable depolarization is found at the positions of the prominent HII regions NGC 604 (RA = $1^{\mathrm{h}}34^{\mathrm{m}}32.9^{\mathrm{s}}$, Dec = 30°47′19.6″), NGC 595 (RA = $1^{\mathrm{h}}33^{\mathrm{m}}32.4^{\mathrm{s}}$, Dec = 30°41′50″) and IC 133 (RA = $1^{\mathrm{h}}33^{\mathrm{m}}15.3^{\mathrm{s}}$, Dec = 30°53′19.7″) as can be expected due to their high densities of thermal electrons. The strongest depolarization in the inner galaxy occurs in the main southern arm I S. No depolarization (DP ≃ 1) is seen on the eastern end of the minor axis and some northern regions.

There are several mechanisms that can lead to wavelength-dependent Faraday depolarization (Burn 1966; Sokoloff et al. 1998). *Differential Faraday rotation* occurs when synchrotron emission originates in a magneto-ionic medium containing a regular magnetic field. The polarization plane of the radiation produced at different depths within the source is rotated over different angles by the Faraday effect and this results in a decrease in the measured degree of polarization. *Faraday dispersion* is depolarization due to fluctuations in the rotation measure within a beam, caused by the turbulent magnetic field and distribution of thermal electrons along the line of sight. When this dispersion is intrinsic to the source, it is called internal Faraday dispersion. In case of a dispersion in an external screen it is called external Faraday dispersion. This depolarization effect may be responsible for the north-south asymmetry in the polarized emission from M 33, if an asymmetry in distribution of the foreground magneto-ionic medium exists. However, as M 33 cannot be resolved in the available foreground surveys, like RM (Johnston-Hollitt et al. 2004) and Hα (Wisconsin Hα mapper) surveys, we do not discuss this depolarization further. Finally *rotation measure gradients* on the scale of the beam or larger due to systematic variation in the regular magnetic field can also lead to depolarization. The regular field in M 33 is not strong enough nor is the inclination of the galaxy high enough for this effect to be significant (in contrast the highly regular field of the strongly inclined galaxy M 31 does produce strong RM gradients, Fletcher et al. 2004).

The depolarization due to internal Faraday dispersion (given by Sokoloff et al. 1998) is

$$\mathrm{DP}_r = \frac{1 - \mathrm{e}^{-2\sigma^2_{\mathrm{RM}}\lambda^4}}{2\sigma^2_{\mathrm{RM}}\lambda^4},$$

$$\sigma_{\mathrm{RM}} = 0.81\langle n_{\mathrm{e}}\rangle\ B_{\mathrm{tur}}\ \sqrt{L\,d/f}, \quad (10)$$

where the dispersion in rotation measure is σ_{RM}, with L the pathlength through the ionized medium, f the filling factor of the Faraday-rotating gas along the line of sight (≃0.5, Beck 2007), and d the turbulent scale (≃50 pc, Ohno & Shibata 1993). Using the Hα emission measure ($EM = \int n_{\mathrm{e}}^2\,\mathrm{d}l$) and a clumping factor $f_{\mathrm{c}} = \langle n_{\mathrm{e}}\rangle^2/\langle n_{\mathrm{e}}^2\rangle$ describing the variations of the electron density, $\langle n_{\mathrm{e}}\rangle$ can be determined by $\langle n_{\mathrm{e}}\rangle = \sqrt{f_{\mathrm{c}}\,EM/L}$. For the local interstellar medium, Manchester & Mebold (1977) found $f_{\mathrm{c}} \simeq 0.05$.

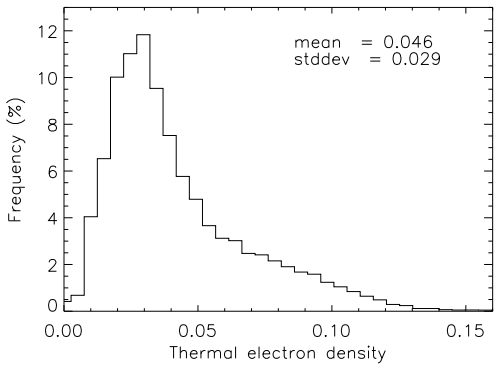

Fig. 10. Histogram of the thermal electron density $\langle n_{\mathrm{e}}\rangle$ (cm^{-3}) distribution across M 33, derived from an extinction corrected Hα (Tabatabaei et al. 2007b). The mean and standard deviation (stddev) of the distribution are also given.

Assuming a thickness of ≃1 kpc for the thermal electrons in the disk of the galaxy (the Galactic value, Cordes & Lazio 2002) and correcting for the inclination of M 33, $L \simeq 1800$ pc. Then the extinction corrected Hα (EM) map of M 33 (Tabatabaei et al. 2007b) generates a distribution of $\langle n_{\mathrm{e}}\rangle$ across the galaxy with a mean value of ≃0.05 cm^{-3} and a most probable value of ≃0.03 cm^{-3} (Fig. 10), that is in agreement with the estimated values in our galaxy (Cordes & Lazio 2002) and other nearby galaxies (Krause et al. 1989; Dumke et al. 2000). Note that a more realistic approach would consider different filling factors and electron densities for the thin and thick disk of the galaxy. However, because the only information we have is a superposition of these components along the line of sight, we are not able to distinguish the role of each component. The resulting $\langle n_{\mathrm{e}}\rangle$ and B_{tur} obtained in Sect. 4.3 (Fig. 8) enable us to estimate DP_r at 3.6 and 20 cm. The lower left panel in Fig. 11 shows the ratio of DP_r at 20 and 3.6 cm.

The other Faraday depolarization effect that is strong in M 33, differential Faraday rotation, is given by Burn (1966) and Sokoloff et al. (1998) as

$$\mathrm{DP}_u = \mathrm{sinc}\ (2\,\mathrm{RM_i}\,\lambda^2), \quad (11)$$

where for simplicity we assume that the disk of M 33 can be represented as a uniform slab. Using the $\mathrm{RM_i}$ map in Fig. 3, we estimated DP_u between 20 and 3.6 cm across the galaxy (Fig. 11, bottom-right). As small variations in $\mathrm{RM_i}$ produce large changes in the sinc function in Eq. (11), the resulting DP_u is not smoothly distributed among neighboring pixels.

Qualitatively, both kinds of Faraday depolarization contribute to the observed depolarization in M 33. The global phenomenon, the north-south asymmetry, is visible in both DP_u as weaker depolarization ($\mathrm{DP}_{20/3} \sim 1$) in the north and also in DP_r as stronger depolarization ($\mathrm{DP}_{20/3} \sim 0$) in the south part of the central region. However, locally e.g. at the positions of HII complexes and the southern spiral arms, DP_r could explain the observed depolarization. The contributions of DP_u and DP_r vary region by region. A more quantitative comparison requires a combination of DP_u and DP_r across the galaxy, but this needs a detailed modelling of depolarization along with distribution of the filling factors f and f_{c}, the pathlength L, and the turbulent scale d across the galaxy.

In the south of M 33, a strong turbulent condition is indicated from the HI line-widths being larger than in the north (Deul & van der Hulst 1987), which could be connected to the high star formation activities in the southern arms, particularly in the main

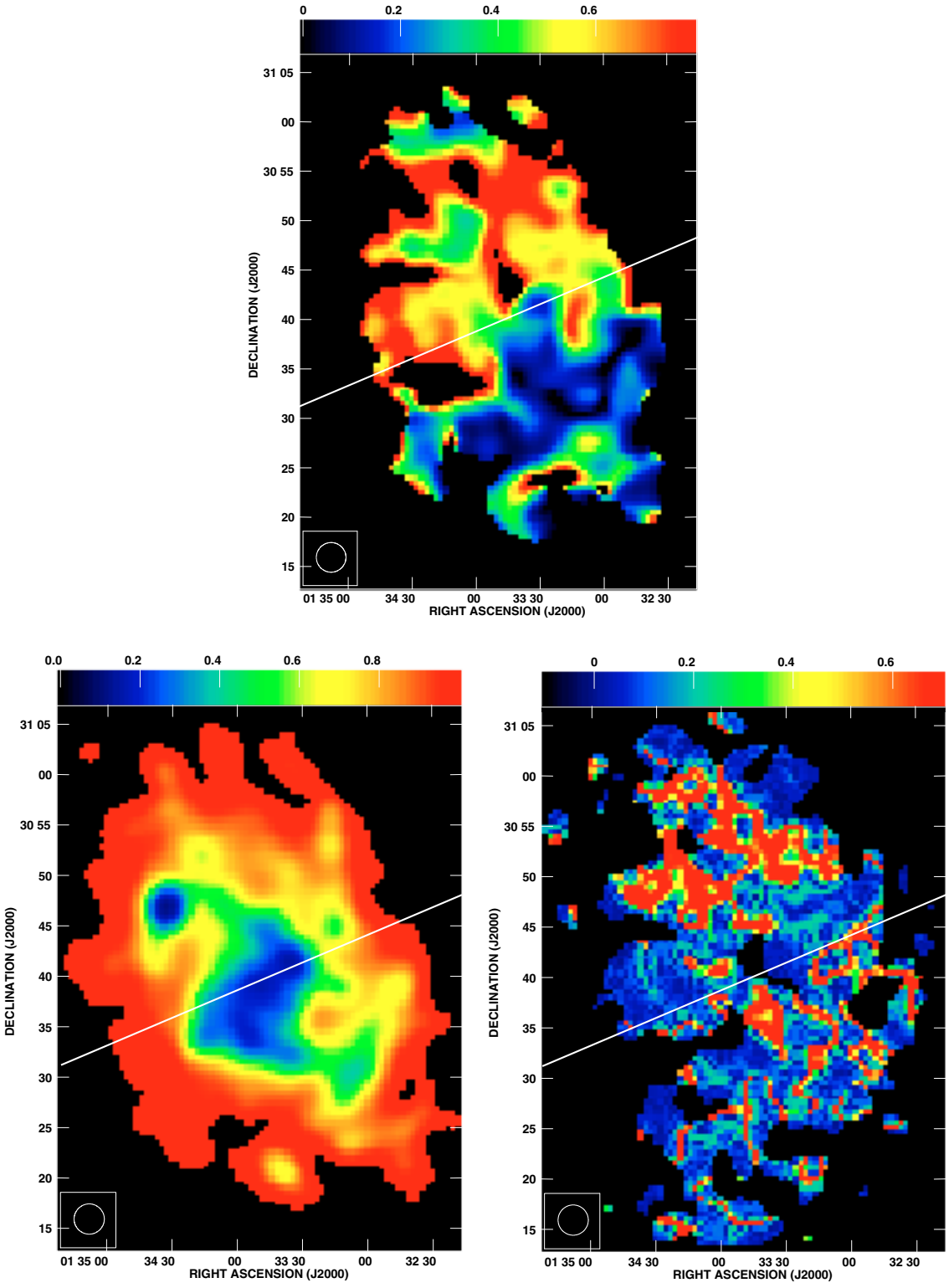

Fig. 11. *Top*: observed depolarization $DP_{20/3}$ between 3.6 and 20 cm (Eq. (9)). *Bottom-left*: estimated depolarization $DP_{20/3}$ due to dispersion in Faraday rotation (Eq. (10)), and *bottom-right*: estimated depolarization $DP_{20/3}$ due to differential Faraday rotation (Eq. (11)). The straight line shows the minor axis of M 33.

arm I S (Tabatabaei et al. 2007c). Hence, we conclude that the highly turbulent conditions in the southern half of M 33 along with a magneto-ionic medium containing vertical regular magnetic fields reduce the degree of polarization of the integral emission from the southern half and cause the wavelength-dependent north-south asymmetry in polarization (or depolarization).

6. Discussion

6.1. Vertical magnetic fields

The model regular magnetic field described in Table 2 and shown in Fig. 7 has a vertical component in each ring. In the inner ring,

the combination of the modes $m = z0$ and stronger $m = z1$ produces a sinusoidal vertical field that is strongest near the major axis: pointing away from us at $\theta \simeq 30°$ and towards us at $\theta \simeq 210°$. In the outer ring the vertical field is also strongest near the major axis, at $\theta \simeq 10°$ (directed away) and $\theta \simeq 190°$ (directed towards).

The presence of a vertical component in the regular magnetic field was indicated locally by our rotation measure maps (Sect. 3). However, the large scale vertical field required by our fits requires a global origin. The strong B_z along the major axis together with the long lines of sight through the magneto-ionic medium on the eastern and western minor axis (Sect. 3) suggest that the galactic warp may play a role. In other words, the "vertical" field that we identify may be due to the severe warp in M 33 (Rogstad et al. 1976; Reakes & Newton 1978; Sandage & Humphreys 1980; Corbelli & Schneider 1997). The inner HI disk investigated by Rogstad et al. (1976) shows a warp beginning at a radius of ≃5 kpc with a change in the inclination angle of 40° at 8 kpc. The warp of the optical plane begins as close to the center as the first arm system at 2 kpc (the center of our inner ring), with a change in the arm inclination of >15° at 3 kpc and 25° at 5 kpc (Sandage & Humphreys 1980). The model in Sect. 4.2 assumes a constant inclination of $i = 56°$ but in a strongly warped disc i varies with radius and azimuth. In this case, even if $B_{\rm reg}$ only has components in the *warped* disk plane $B_{\rm d}$, as for e.g. M 51 (Berkhuijsen et al. 1997), M 31 (Fletcher et al. 2004), and NGC 6946 (Beck 2007), there will be an *apparent* vertical component $\hat{B}_z$ (as well as an apparent disk parallel component $\hat{B}_{\rm d}$) with respect to the *average* disk-plane.

The ratio $\hat{B}_z/\hat{B}_{\rm d} = \tan i_w$ where i_w is the warp inclination. So for $w_i \simeq 15°$ in the inner ring $\hat{B}_z/\hat{B}_{\rm d} \simeq 0.3$ and in the outer ring $w_i \simeq 25°$ gives $\hat{B}_z/\hat{B}_{\rm d} \simeq 0.5$. Our model field in Table 2 has $B_z/B_{\rm d} \leq 2 \pm 1$ in the 1−3 kpc ring and $B_z/B_{\rm d} \leq 1.0 \pm 0.4$ in the 3−5 kpc ring. This indicates that, in the outer ring, the vertical field could be mainly due to the warp. However, a real vertical field of a broadly comparable strength to the disk field can exist in the inner ring.

6.2. Magnetic and spiral-arm pitch angles

The pitch angles of the horizontal component of the regular magnetic field are high: $p_{\rm B} = 48°$ in the 1−3 kpc ring and $p_{\rm B} = 42°$ in the 3−5 kpc ring. These magnetic field pitch angles are however lower than the pitch angles of the optical arm segments identified by Sandage & Humphreys (1980), which are typically $p_{\rm a} = 60°$−$70°$. A combination of shear from the differential rotation, producing an azimuthal magnetic field with $p_{\rm B} = 0°$, and compression in spiral arm segments, amplifying the component of the field parallel to the arms $p_{\rm B} = 65°$, may be responsible for the observed $p_{\rm B} \simeq 40°$. However, this type of alternate stretching and squeezing of the field could not produce the $m = 0$ azimuthal mode that is found in both rings, unless the pre-galactic field was of this configuration. The presence of a significant $m = 0$ azimuthal mode of $B_{\rm reg}$ can be explained if a large-scale galactic dynamo is operating in M 33: the axisymmetric mode has the fastest growth rate in disk dynamo models (e.g. Beck et al. 1996). This does not mean that a dynamo is the origin of *all* of the regular magnetic field structure in M 33. In particular it would be a strange coincidence if the large $p_{\rm B}$, higher than the typical $p_{\rm B}$ in other disc galaxies by a factor of ∼2, is not connected to the open spiral arms with $p_{\rm a} \simeq 65°$.

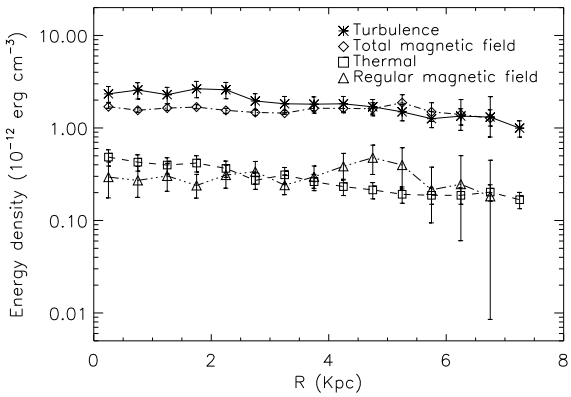

Fig. 12. Energy densities and their variations with galactocentric radius in M 33.

A rough estimate of the magnetic field pitch angles expected due to a simple mean-field dynamo can be obtained by considering the ratio of the alpha-effect – parameterizing cyclonic turbulence generating the radial field B_r from the azimuthal B_θ – to the omega-effect – describing differential rotation shearing the radial field into an azimuthal one. This can be written as (Shukurov 2004)

$$\tan p_{\rm B} = \frac{B_r}{B_\theta} \simeq \frac{1}{2}\sqrt{\frac{\pi\alpha}{hG}}, \qquad (12)$$

where α is a typical velocity of the helical turbulence, h is the scale height of the dynamo active layer and $G = R\,{\rm d}\Omega/{\rm d}R$ gives the shear rate due to the angular velocity Ω. Using the HI rotation curve derived by Corbelli & Salucci (2007), $\alpha \sim 1$ km s^{-1} as a typical value (Ruzmaikin et al. 1988), and an HI scale height of 250 pc at $R = 2$ kpc increasing steadily to 650 pc at $R = 5$ kpc (Baldwin 1981) we obtain approximate pitch angles of $p_{\rm B} \simeq 20°$ and $p_{\rm B} \simeq 15°$ for the 1−3 and 3−5 kpc rings, respectively. These are only about 1/2 to 1/3 of the fitted pitch angles of the $m = 0$ modes. Models specific to M 33, which allow for dynamo action as well as the large scale gas-dynamics of the galaxy, are required to understand the origin of the large $p_{\rm B}$ as well as the vertical component of the regular magnetic field.

6.3. Energy densities in the ISM

The energy densities of the equipartition magnetic fields in the disk ($B_{\rm t}^2/8\pi$ and $B_u^2/8\pi$ for the total and regular magnetic fields, respectively) are shown in Fig. 12. The thermal energy density of the warm ionized gas, $\frac{3}{2}\langle n_{\rm e}\rangle kT_{\rm e}$, is estimated from the Hα map assuming $T_{\rm e} \simeq 10^4$ K (see also Sect. 5). Assuming the pressure equilibrium between the warm and hot ionized gas with $T_{\rm e} \simeq 10^6$ K and an electron density of $\simeq 0.01\langle n_{\rm e}\rangle$ (e.g. Ferrière 2001), the energy density of the hot ionized gas is about the same order of magnitude as the warm ionized gas energy density. For the neutral gas, we derive the energy density of $\frac{3}{2}\langle n\rangle kT$ using the average surface density of total (molecular + atomic) gas given by Corbelli (2003) and an average temperature of $T \simeq 50$ K (Wilson et al. 1997). The warm neutral gas with a typical temperature of ≃6000 K has roughly the same thermal energy density as the cold neutral gas, due to a ≃100 times lower density (e.g. Ferrière 2001). Assuming a constant scale height of the disk of 100 pc (as used for NGC 6946 Beck 2007), we obtain a gas density of $\langle n\rangle \simeq 6$ cm^{-3} at $R = 1$ kpc (that is about 8 times lower than the corresponding value in NGC 6946) to ≃2 cm^{-3} at

R = 5 kpc (about 3.5 times lower than that in NGC 6946)[5]. The total thermal energy density shown in Fig. 12 includes the contribution of the warm, hot ionized and the cold, warm neutral gas. Figure 12 also shows the kinetic energy density of the turbulent motion of the neutral gas estimated using a turbulent velocity of 10 km s^{-1} (Corbelli & Schneider 1997; Milosavljević 2004).

Generally, the energy densities of all components are about the same order of magnitude as in the Milky Way (Cox 2005), but one order of magnitude smaller than in NGC 6946 (Beck 2007). The low thermal energy density compared to the total magnetic field energy density shows that the M 33 ISM is a low β plasma (β is defined as the thermal to magnetic energy density ratio; similar results were found in the Milky Way and NGC 6946 Cox 2005; Beck 2007). On the other hand, the low thermal energy density compared to that of the turbulent motion indicates that turbulence in the diffuse ISM is supersonic (as in NGC 6946 Beck 2007). This is in agreement with 3D MHD models for the ISM (de Avillez & Breitschwerdt 2007).

The energy densities of the total magnetic field and turbulent gas motion are about the same. This hints at the generation of interstellar magnetic fields from turbulent gas motion for $R < 8$ kpc in M 33. For a comparison at larger radii, detection of the magnetic fields is required using deep surveys of Faraday rotation of polarized background sources. This seems to be promising as the scale length of the total magnetic field (≃24 kpc, Tabatabaei et al. 2007b) is much larger than the present detection limit of the radio emission.

The energy density of the regular field is about 3−7 times smaller than that of the total field. Furtheremore, it shows more variation with radius than the total field strength, with a maximum increase at $4.5 < R < 5.5$ kpc.

6.4. Comparison with M 31

Comparing magnetic fields in our neighbors, M 33 and M 31, is instructive especially because a similar method was used to find the 3D magnetic field structure in both galaxies. It is interesting to see that the total magnetic field strength is about the same in M 33 and M 31 (≃7 μG), but the regular field strength in M 33 is about half of that in M 31 (≃4 μG). Furthermore, in contrast to M 33, M 31 has a disk plane parallel regular field without a vertical component. In other words, the large-scale magnetic field is well-ordered and strong relative to the small-scale field in M 31. The regular magnetic field is fitted by a dominant $m = 0$ mode in M 31 (Fletcher et al. 2004) that is much stronger than that in M 33.

The larger pitch angles of the horizontal magnetic field in M 33 than in M 31 is not due to a smaller shear in M 33. From their rotation curves (Carignan et al. 2006; Corbelli & Salucci 2007), we see that the shear rate at the relevant radii is higher in M 33 (>10 km s^{-1} kpc^{-1} at $1 < R < 5$ kpc) than in M 31 (≃6 km s^{-1} kpc^{-1} at $8 < R < 12$ kpc).

The fact that M 33 has a higher star formation efficiency than its 10-times more massive neighbor, M 31, may be a clue to the origin of their differences. Strong star formation activities in the inner part of M 33 could cause vertical distribution of magneto-ionic matter and hence the vertical magnetic field. Furthermore, stronger turbulence in the interstellar medium generally can be caused by a high star formation rate increasing the dynamo alpha-effect and hence providing large pitch angles of the horizontal magnetic field.

[5] Hence, the radial profile of the energy density of the neutral gas is much flatter in M 33 than in NGC 6946 (see Fig. 5 in Beck 2007).

7. Summary

The distributions of linearly polarized intensity and polarization angle at 3.6, 6.2, and 20 cm along with the maps of nonthermal intensity and nonthermal spectral index (obtained from the new separation method, Tabatabaei et al. 2007b) yielded high-resolution distributions of RM, nonthermal degrees of polarization, and Faraday depolarization in M 33. Furthermore, we derived the 3D structure of the regular magnetic field by fitting the observed azimuthal distributions of the polarization angle within two rings of 2 kpc width in the radial range 1 to 5 kpc. The main results and conclusions are as follows:

1. The average nonthermal degree of polarization is $P_{\rm nth} \simeq 10\%$ (at 3.6 cm) for $R < 7.5$ kpc and >20% in parts of the magnetic filament. Due to Faraday depolarization $P_{\rm nth}$ decreases to ≃6% at 20 cm.
2. The intrinsic Faraday rotation shows larger small-scale variations and a weaker correlation with PI in the south than in the north of M 33. The higher star formation activity in the southern arms could increase the turbulent velocity of interstellar clouds and disturb the regular field configuration. On the other hand, a good correlation between RM$_{\rm i}$ and PI in the magnetic filament in the north-west of M 33 shows that here the magnetic field is mainly regular.
3. The average equipartition strengths of the total and regular magnetic fields are $B_{\rm tot} \simeq 6.4\,\mu$G and $B_{\rm reg} \simeq 2.5\,\mu$G for $R < 7.5$ kpc. The regular magnetic field strength is higher within the ring at $4.5 < R < 5.5$ kpc, which contains the magnetic filament that has a maximum regular field of $B_{\rm reg} \simeq 6.6\,\mu$G. Strong turbulent magnetic fields ($B_{\rm tur} > 7\,\mu$G) occur in the extended central region and the arms I S and part of II S.
4. The 3D structure of the regular magnetic field can be explained by a combination of azimuthal modes of $m = 0+z0+z1$ in the 1−3 kpc ring and $m = 0+1+z1$ in the 3−5 kpc ring. The horizontal magnetic field component follows an arm-like pattern with pitch angles smaller than those of the optical arm segments, indicating that large-scale gas-dynamical effects such as compression and shear are not solely responsible for the spiral magnetic lines. The significant axisymmetric mode ($m = 0$) in both rings indicates that galactic dynamo action is present in M 33.
5. The presence of vertical magnetic fields, shown by the best-fit model of the 3D field structure ($z1$) and indicated by the Faraday rotation distribution across the galaxy, is possibly due to both global (e.g. M 33's warp or interaction with M 31) and local (e.g. star formation activities, Parker loops) phenomena. The warp can better explain the origin of the vertical field in the outer ring (3−5 kpc).
6. In the southern half of M 33, an excess of differential Faraday rotation together with strong Faraday dispersion seem to be responsible for the north-south asymmetry in the observed depolarization (which is wavelength dependent).
7. The energy densities of the magnetic field and turbulence are about the same, confirming the theory of generation of interstellar magnetic fields from turbulent gas motion. Furthermore, it seems that the ISM in M 33 can be characterized by a low β plasma and dominated by a supersonic turbulence, as the energy densities of the magnetic field and turbulence are both higher than the thermal energy density.

Acknowledgements. We are grateful to E. M. Berkhuijsen, U. Klein and E. Krügel for valuable and stimulating comments. F.T. was supported through a stipend from the Max Planck Institute for Radio Astronomy (MPIfR). A.F. thanks the Leverhulme Trust for financial support under research grant F/00 125/N.

References

Baldwin, J. E. 1981, in Structure and Evolution of Normal Galaxies, ed. S. M. Fall, & D. Lynden-Bell, 137
Beck, R. 1979, Ph.D. Thesis, Rheinische Friedrich-Wilhelms-Universitaet, Bonn
Beck, R. 2007, A&A, 470, 539
Beck, R., & Krause, M. 2005, Astron. Nachr., 326, 414
Beck, R., Brandenburg, A., Moss, D., Shukurov, A., & Sokoloff, D. 1996, ARA&A, 34, 155
Berkhuijsen, E. M., Horellou, C., Krause, M., et al. 1997, A&A, 318, 700
Broten, N. W., MacLeod, J. M., & Vallee, J. P. 1988, Ap&SS, 141, 303
Buczilowski , U. R., & Beck, R. 1991, A&A, 241, 47
Burn, B. J. 1966, MNRAS, 133, 67
Carignan, C., Chemin, L., Huchtmeier, W. K., & Lockman, F. J. 2006, ApJ, 641, L109
Corbelli, E. 2003, MNRAS, 342, 199
Corbelli, E., & Salucci, P. 2007, MNRAS, 374, 1051
Corbelli, E., & Schneider, S. E. 1997, ApJ, 479, 244
Cordes, J. M., & Lazio, T. J. W. 2002, ArXiv Astrophysics e-prints
Cox, D. P. 2005, ARA&A, 43, 337
de Avillez, M. A., & Breitschwerdt, D. 2007, ApJ, 665, L35
Deul, E. R., & van der Hulst, J. M. 1987, A&AS, 67, 509
Dumke, M., Krause, M., & Wielebinski, R. 2000, A&A, 355, 512
Ferrière, K. M. 2001, Rev. Mod. Phys., 73, 1031
Fletcher, A., Berkhuijsen, E. M., Beck, R., & Shukurov, A. 2004, A&A, 414, 53
Johnston-Hollitt, M., Hollitt, C. P., & Ekers, R. D. 2004, in The Magnetized Interstellar Medium, ed. B. Uyaniker, W. Reich, & R. Wielebinski, 13
Krause, M. 1990, in Galactic and Intergalactic Magnetic Fields, ed. R. Beck, R. Wielebinski, & P. P. Kronberg, IAU Symp., 140, 187
Krause, M., Hummel, E., & Beck, R. 1989, A&A, 217, 4
Manchester, R. N., & Mebold, U. 1977, A&A, 59, 401
Milosavljević, M. 2004, ApJ, 605, L13
Ohno, H., & Shibata, S. 1993, MNRAS, 262, 953
Reakes, M. L., & Newton, K. 1978, MNRAS, 185, 277
Reich, W. 2006, ArXiv Astrophysics e-prints
Rogstad, D. H., Wright, M. C. H., & Lockhart, I. A. 1976, ApJ, 204, 703
Ruzmaikin, A. A., Sokolov, D. D., & Shukurov, A. M. 1988, Magnetic fields of galaxies, Chapter VI.4, Astrophys. Space Sci. Library, 133
Sandage, A., & Humphreys, R. M. 1980, ApJ, 236, L1
Segalovitz, A., Shane, W. W., & de Bruyn, A. G. 1976, Nature, 264, 222
Shukurov, A. 2004, ArXiv Astrophysics e-prints
Simard-Normandin, M., & Kronberg, P. P. 1980, ApJ, 242, 74
Sokoloff, D. D., Bykov, A. A., Shukurov, A., et al. 1998, MNRAS, 299, 189
Tabara, H., & Inoue, M. 1980, A&AS, 39, 379
Tabatabaei, F. S., Beck, R., Krause, M., Krügel, E., & Berkhuijsen, E. M. 2007a, Astron. Nachr., 328, 636
Tabatabaei, F. S., Beck, R., Krügel, E., et al. 2007b, A&A, 475, 133
Tabatabaei, F. S., Krause, M., & Beck, R. 2007c, A&A, 472, 785
Wilson, C. D., Walker, C. E., & Thornley, M. D. 1997, ApJ, 483, 210